

Uncertainties in historical changes and future projections of drought. Part I: estimates of historical drought changes

Aiguo Dai^{1,2} · Tianbao Zhao³

Received: 5 November 2015 / Accepted: 18 May 2016
© Springer Science+Business Media Dordrecht 2016

Abstract How drought may change in the future are of great concern as global warming continues. In Part I of this study, we examine the uncertainties in estimating recent drought changes. Substantial uncertainties arise in the calculated Palmer Drought Severity Index (PDSI) with Penman-Monteith potential evapotranspiration (PDSI_{pm}) due to different choices of forcing data (especially for precipitation, solar radiation and wind speed) and the calibration period. After detailed analyses, we recommend using the Global Precipitation Climatology Centre (GPCC) or the Global Precipitation Climatology (GPCP) datasets over other existing land precipitation products due to poor data coverage in the other datasets since the 1990s. We also recommend not to include the years after 1980 in the PDSI calibration period to avoid including the anthropogenic climate change as part of the natural variability used for calibration. Consistent with reported declines in pan evaporation, our calculated potential evapotranspiration (PET) shows negative or small trends since 1950 over the United States, China, and other regions, and no global PET trends from 1950 to 1990. Updated precipitation and streamflow data and the self-calibrated PDSI_{pm} all show consistent drying during 1950–2012 over most Africa, East and South Asia, southern Europe, eastern Australia, and many parts of the Americas. While these regional drying trends resulted primarily from precipitation changes

This article is part of a Special Issue on “Decadal Scale Drought in Arid Regions” edited by Zong-Liang Yang and Zhuguo Ma.

Electronic supplementary material The online version of this article (doi:10.1007/s10584-016-1705-2) contains supplementary material, which is available to authorized users.

✉ Aiguo Dai
adai@albany.edu

¹ Department of Atmospheric and Environmental Sciences, University at Albany, SUNY, Albany, New York 12222, USA

² National Center for Atmospheric Research, Boulder, CO, USA

³ Key Laboratory of Regional Climate-Environment Research for East Asia, Institute of Atmospheric Physics (IAP), Chinese Academy of Sciences (CAS), Beijing, China

related to multi-decadal oscillations in Pacific sea surface temperatures, rapid surface warming and associated increases in surface vapor pressure deficit since the 1980s have become an increasingly important cause of widespread drying over land.

Keyword Drought · PDSI · Precipitation · Historical drought change · Uncertainties · Streamflow

1 Introduction

Drought is among the costliest natural disasters due to its long duration and lasting effects on agriculture and other sectors, and its low predictability among all extreme weather and climate events (Wilhite 2000; Mishra and Singh 2010). During recent years, many regions have experienced frequent severe droughts, such as the 2005 and 2010 Amazon droughts (Marengo et al. 2008; Lewis et al. 2011), the 2009–2011 winter-spring drought in southern China (Barriopedro et al. 2012; Sun and Yang 2012), the Southwest North American drought since 2010 (Peterson et al. 2012; Hoerling et al. 2012), the Horn of Africa and Sahel droughts in 2011 (Lyon and DeWitt 2012), the recent decade-long drought in Australia (McGrath et al. 2012), and the on-going record-breaking drought in California since 2012 (Williams et al. 2015). Although natural variability is often the primary cause for individual drought events, the increased frequency of severe droughts during recent years over the Americas and other regions is consistent with model-projected increases in drought frequency and severity over these regions under increasing greenhouse gases (GHGs) (Wang 2005; Burke et al. 2006; Seager et al. 2007; Sheffield and Wood 2008; Dai 2011a, 2013a; Wehner et al. 2011; Taylor et al. 2013; Feng and Fu 2013; Cook et al. 2014; Prudhomme et al. 2014; Scheff and Frierson 2015; Zhao and Dai 2015). For future drought increases, increases in atmospheric demand for moisture associated with rising temperatures (Feng and Fu 2013; Scheff and Frierson 2014) are the primary cause, with decreasing precipitation enhancing the drying over subtropical land areas (Zhao and Dai 2015). For historical drought increases since the 1970s (Dai 2011b, 2013a), decreasing precipitation is the primary cause over most areas, although increased atmospheric demand associated with rising temperatures since the 1980s is also a significant contributor. As analyzed below (section 5), these historical changes are not inconsistent with the reported declines in pan evaporation over the contiguous United States, China, India, and other regions (McVicar et al. 2012).

While all the studies mentioned above show considerable future drying in the twenty-first century, the estimated historical drying extent and magnitude since 1950 differ significantly among some studies. In particular, Sheffield et al. (2012) found only small drying over global land from 1950 to 2008 solely based on their calculated Palmer Drought Severity Index (PDSI; Palmer 1965) with the Penman-Monteith potential evapotranspiration (PET) (PDSI_{pm}). This is in contrast to the conclusions made by Dai et al. (2004), Trenberth et al. (2007), Dai (2011a, 2011b), and Dai (2013a), who analyzed the changes in various forms of the PDSI as well as historical precipitation and streamflow records and concluded that the warming since the 1980s has enhanced the drying over many land areas. Van der Schrier et al. (2013) concluded that different calibration periods used in calculating the PDSI can explain a portion of the differences in the estimated PDSI trends. Trenberth et al. (2014) showed that the popular Climatic Research Unit (CRU) precipitation dataset (TS 3.10.01 or older versions) used by Sheffield et al. (2012), van der Schrier et al. (2013), IPCC (2007, 2013), and many other studies (but not by Dai et al.), has a wet bias compared with other products since the 1990s due

to a sharp decline in its number of rain-gauges for the recent decades. Trenberth et al. (2014) suggested that this could be a major factor for the different PDSI trends found by Dai et al. and Sheffield et al.

In this study, we further examine the uncertainties in estimating historical drying trends and the key factors that may have contributed to the different conclusions made by Sheffield et al. (2012) and by Dai et al. (2004) Dai (2011a, 2011b), and Dai (2013a). We also provide an analysis of updated precipitation and streamflow data and the calculated self-calibrated PDSI_{pm} (sc_PDSI_{pm}) to assess historical aridity trends from 1950 to 2014. Furthermore, we analyze our calculated PET to assess whether our PET and thus the sc_PDSI_{pm} are consistent with the reported declines in pan evaporation (McVicar et al. 2012), a proxy of PET. Here, we focus on the uncertainties in the sc_PDSI_{pm} associated with issues in precipitation datasets, and did not explore the impact of the uncertainties in the other forcing data mainly because there do not exist reliable data to make such an assessment. In part II of this study (Zhao and Dai 2016), the historical drought changes are compared with climate model-simulated response to historical CO₂ and other external forcing.

In the following, we describe the data and method in section 2. Section 3 discusses the main sources of uncertainty in estimating historical drought changes based on the sc_PDSI_{pm}. An update analysis of drought changes since 1950 is presented in section 4. A summary is given in section 5.

2 Data and method

The PDSI (Palmer 1965) and its variants are one of the popular drought indices used to quantify variations and long-term changes in drought and aridity on global (Dai et al. 1998, 2004; Dai 2011a, 2011b, 2013a; van der Schrier et al. 2011, 2013; Sheffield et al. 2012) and regional scales (Zhai et al. 2010; van der Schrier et al. 2007; Wei and Wang 2013). In particular, the self-calibrated PDSI (Wells et al. 2004) with Penman-Monteith potential evapotranspiration (sc_PDSI_{pm}) (Dai 2011b; van der Schrier et al. 2011) overcomes some main caveats in the original PDSI, and thus is considered as a more reliable index for quantifying long-term drought changes, primarily for agricultural drought in response to global warming (Dai 2011b; Zhao and Dai 2015).

However, the calculated sc_PDSI_{pm} (or PDSI_{pm}) may contain large uncertainties due to a lack of reliable forcing data for historical precipitation, solar radiation and other near-surface meteorological fields that are needed for computing the sc_PDSI_{pm} (Dai 2011b). To address this problem, we first examine some key issues in calculating the sc_PDSI_{pm}. This includes evaluation of the existing precipitation products and a proper choice of the calibration period for computing the sc_PDSI_{pm}. We then compare the change patterns in the sc_PDSI_{pm} with observed changes in precipitation (a measure of meteorological drought) and streamflow or runoff (a measure of hydrologic drought) to assess whether the changes in these different drought measures are qualitatively consistent with each other in terms of the spatial patterns of change. Consistent change patterns among these different but physically-related drought measures can provide a more reliable assessment of historical drought trends than using one measure alone.

We updated monthly sc_PDSI_{pm} data to December 2014 using the method and forcing data described in Dai (2011b), with modifications described in Supplementary Materials (SM).

Drought often leads to warmer temperatures and lower relative humidity, which in turn raise PET. Higher PET enhances drought, thereby creating a positive feedback.

3 Uncertainties in historical forcing data

As mentioned in Introduction, Sheffield et al. (2012) found little drying from 1950 to 2008 over global land based on their calculated PDSI_{pm} using their meteorological forcing data, which were largely based on the NCEP/NCAR reanalysis data with the monthly mean T and P adjusted to match those of the CRU TS3.10. The CRU TS3.10 P contained a bug and it was soon replaced by CRU TS3.10.01 (see <http://www.cru.uea.ac.uk/cru/data/hrg/#legacy>). Sheffield et al. (2012) realized that there exist large uncertainties in datasets for precipitation and net surface radiation, and used four precipitation datasets (CRU TS3.10, DaiP, GPCC V4, and WilP) and two radiation estimates to generate an ensemble mean PDSI_{pm} and its uncertainty range. In doing so, they implicitly assumed that all the available datasets were equally likely to be true. As shown below, there is strong evidence to suggest otherwise, that is, some of the P data sets are likely to be more reliable than others and thus they should be used.

In contrast, Dai (2011b) used the DaiP, CRU T data, and observed cloudiness-based estimates of surface radiation, plus surface wind, humidity and air pressure data from the same NCEP/NCAR reanalysis. Another difference is that Dai (2011b) used a 30-year (1950–1979) period while Sheffield et al. (2012) used the whole analysis period (1950–2008) as the calibration period in calculating the PDSI. One advantage of using the whole analysis period as the calibration period, as noticed by van der Schrier et al. (2013), is that it includes all the variations and changes in the data and thus will ensure the PDSI values over the whole analysis period within a range (approx. -6 to +6) as envisioned originally by Palmer (1965), and thus Palmer's classification ranges can be used to define various types of drought. However, because we are dealing with a changing climate with a focus on long-term changes rather than classifying drought types, we should not choose a calibration period solely based on this consideration.

The period since the 1980s has a clear warming trend that has been attributed mainly to anthropogenic forcing, rather than natural climate variations (IPCC 2007, 2013). Because of this, it is inappropriate to include this trend in the variance used to calibrate the PDSI values. Doing so would effectively reduce the PDSI value range and its trend magnitude. One extreme example would be to use the whole analysis period from 1950 to 2099 as the calibration period in computing the PDSI for model-simulated historical and future climates. This would effectively reduce the future PDSI change magnitude (with little effect on its temporal evolution) and be equivalent to assume the 1950–2099 mean as the norm that we should calibrate with. Obviously, that is incorrect.

As shown by van der Schrier et al. (2013), using different calibration periods may account for some of the PDSI trend differences between Dai (2011b) and Sheffield et al. (2012), while the discontinuity error around 2004/2005 in Dai (2011b)'s forcing data is unlikely to be a major factor. To further quantify the effects of these issues, we compare the global-mean time series of the sc_PDSI_{pm} from Dai (2011b) and that without the discontinuity error (Fig. 1a), and the sc_PDSI_{pm} calculated separately with 1950–1979 (as in Dai 2011b) and 1950–2008 (as in Sheffield et al. 2012) as the calibration period for the different precipitation cases (Fig. 1b). It is clear that the difference caused by the discontinuity error around 2005, which is similar to that shown in Sheffield et al. (2012), changes the overall trend from 1950 to 2008 only slightly from about -0.8 to -0.9 change per century, with both being statistically significant. Thus, while this error may have slightly enhanced (by ~10 %) the drying trend in the sc_PDSI_{pm} used by Dai (2011b), it certainly has no effect on the downward trend up to

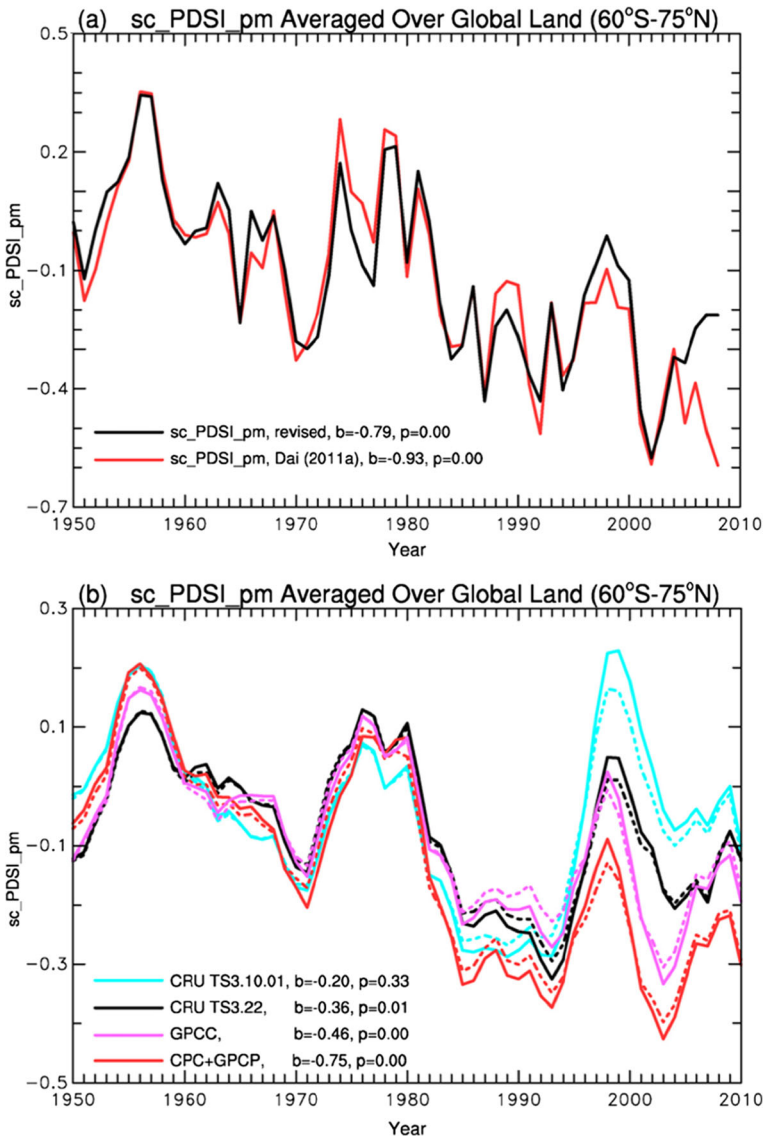


Fig. 1 a Annual time series from 1950 to 2008 of globally (60°S-75°N) averaged sc_PDSI_pm from Dai (2011b) (red) and from a revised version (black) without the discontinuity error around 2005. b Globally (60°S-75°N) averaged and 5-year smoothed sc_PDSI_pm time series from 1950 to 2010 calculated using the same meteorological forcing data (from CRU TS 3.22) except for precipitation, which was from CRU TS3.10.01 (blue), CRU TS3.22 (black), GPCC V6 (pink), and CPC + GPCP (red). The solid lines are for the case using 1950–1979 as the calibration period while the dashed lines are derived using 1950–2008 as the calibration period. In both panels, the linear trend (b , in changes per 100 years) and its attained p -value (p) are also shown (for the solid lines only in panel b). The slope b (p -value) for the dashed lines are -0.24 (0.19) for CRU TS 3.10.01, -0.35 ($p = 0.01$) for CRU TS3.22, -0.42 ($p < 0.01$) GPCC, and -0.72 ($p < 0.01$) for CPC + GPCP (DaiP). Autocorrelation was considered in computing the p -value by reducing the effective degrees of freedom based on Zhao and Khalil (1993)

2004 and also cannot explain the difference between the results of Dai (2011b) and Sheffield et al. (2012), who essentially discarded the results of Dai (2011b) using this discontinuity error as the main reason.

As expected, using 1950–2008 (instead of 1950–1979) does reduce the variation range and trend magnitude of the *sc_PDSI_pm*, but only slightly, e.g., from -0.75 to -0.68 change per century for the DaiP case (Fig. 1b). Thus, the difference in the calibration period is also not a major factor, although we consider 1950–1979 as a better choice based on the arguments presented above.

As shown in Sheffield et al. (2012) and Trenberth et al. (2014), large uncertainties exist in current estimates of historical precipitation changes over global land due to sparse observations and data quality issues (Dai et al. 1997). In particular, the CRU TS 3.10 and TS 3.10.01 datasets had poor gauge coverage since the 1990s, with only about 1500 gauges after year 2000. In comparison, GPCC V6 has $\sim 10,000$ gauges after 2000 (see Fig. 1 of Trenberth et al. 2014). The GPCP v2.2 (used in DaiP) has similar raingauge coverage as the GPCC product. Fig. S1 in SM illustrates the large differences in the rain-gauge density and coverage between CRU TS3.10.01 and GPCC V6. The use of vastly more observations in GPCC V6, instead of filling the gaps with data from far away stations or with 1961–1990 climatology (as done in the CRU TS datasets), should greatly improve the reliability of the GPCC V6 data, especially for the recent decades. In fact, with improved raingauge coverage, the updated CRU TS3.21 P data show lower global-mean land precipitation since the 1990s than the CRU TS3.10.01 and are closer to GPCC V6 and GPCP v2.2 (Trenberth et al. 2014). The fact that adding more gauges to CRU TS3.10.01 makes it closer to GPCC V6 and GPCP v2.2 suggests that the estimates from GPCC V6 and GPCP v2.2 are likely to be closer to the truth than the CRU TS3.10.01 (while CRU TS3.10 P should not be used). Unfortunately, GPCC does not release its station data to the scientific community.

Another way to evaluate the various precipitation products is to compare their correlations (or the correlations of the PDSI derived from the P products) with physically related but independently measured quantities, such as soil moisture, streamflow, and GRACE satellite-observed water storage changes (Swenson 2012), as we have done previously (e.g., Dai et al. 2004; Dai 2011b). Fig. S2 in SM shows an example of such comparison, with Fig. S2a showing the GRACE vs. *sc_PDSI_pm* monthly anomaly correlation during April 2002–December 2012 for DaiP (i.e., GPCP v2.2) case and the difference from Fig. S2a in the other panels for the GPCC V6, CRU TS3.22, and WilP cases. It is clear that the correlations are strong ($r \geq 0.6$) and similar among the four products over the central and eastern U.S., Europe and other areas with good gauge coverage, thus confirming the reliability of the water storage variations represented by the GRACE data. However, over Africa, South America, central and South Asia, and other regions with poor gauge coverage (Fig. S1), the CRU TS3.22 (similar for CRU TS3.10.01), WilP and even the GPCC V6 product generally show lower correlations than the GPCP data. One exception is central Africa (south of the equator) where the CRU and WilP data show higher correlations with the GRACE data. Despite this, Fig. S2 suggests that recent variations and changes in global land precipitation since the 1990s are likely to be more reliable in the GPCP v2.2 and GPCC V6 datasets than the CRU TS 3.10.01 and CRU TS3.22 (and the WilP) datasets, simply because the rain-gauge coverage is too poor in the latter datasets for the recent decades. Thus, it is unwise to simply treat these P datasets equally and use the ensemble mean of the *PDSI_pm* derived from them as the best estimate, as is done in Sheffield et al. (2012).

As shown by Trenberth et al. (2014), the wet bias in the CRU TS3.10.01 P data since the 1990s resulted in considerably higher global-mean *sc_PDSI_pm* for the recent decades compared with the cases using the DaiP, GPCC V6, and WilP P data. Figure 1b further shows that the updated CRU TS3.22 (with more gauges but still substantially fewer than GPCC V6,

Trenberth et al. 2014) makes the *sc_PDSI_pm* closer to the other cases and the 1950–2010 drying trend becomes statistically significant as with the other cases.

Significant differences also exist in other forcing data between ours (Fig. S3 in SM) and those of Sheffield et al. (2012). In particular, global-land downward surface solar radiation in Sheffield et al. (2012) shows a large decline ($\sim 4\text{Wm}^{-2}$) from about 1970 to 1976, and their surface wind speed also shows spurious variations with different variance before and after around 1980 and a downward trend (see their Fig. S5), although surface observations (which often contain spurious discontinuities) do show some stilling (McVicar et al. 2012). These large changes in solar radiation and surface wind speed should both reduce evapotranspiration and thus increase *PDSI_pm* for the recent decades. In contrast, our cloudiness-based estimate of solar radiation and the 20CR wind data (Fig. S3) do not contain such large long-term changes. We realize that our solar radiation estimates do not include the effects of aerosol changes; however, the large drop in the early 1970s and other long-term changes in Sheffield et al.'s solar radiation estimates do not match the evolution of aerosol-induced radiative forcing (Myhre et al. 2013), which shows increasing cooling effects globally from 1950 to 1990 but declining effects after 1990. The 20CR (Compo et al. 2011) assimilated observed surface pressure and sea surface temperatures (SSTs) (while surface observations besides SSTs were not assimilated in the NCEP/NCAR reanalysis), thus the 20CR surface winds are likely to be reliable for air pressure-induced changes, but unable to account for land surface and other changes.

4 An updated analysis of drought trends since 1950

The calculated *sc_PDSI_pm* (a measure of agricultural drought) is just one of many drought measures available (Dai 2011a). The conclusions made by Dai et al. (2004); Dai (2011a, 2011b) and Dai (2013a) were based not only on the *PDSI* trends, but also changes in observed precipitation (a measure of meteorological drought) and streamflow (a measure of hydrologic drought). Figure 2 compares trend maps for 1950–2012 using the DaiP precipitation data (broadly similar for GPCC V6 and CRU TS 3.22), runoff inferred from downstream streamflow gauge records (Dai et al. 2009; Dai 2016), and our *sc_PDSI_pm* (based on the DaiP and other forcing data described in section 2). The focus here is on the broad spatial patterns of the trends, as these are physically related but different variables. Some similarity is expected between the *P* and *sc_PDSI_pm* change patterns since the *P* data are a major driver of the *sc_PDSI_pm*, which also includes the effects of other meteorological fields (Fig. S3). However, the runoff changes are derived from independently measured streamflow rates. Thus, consistent trend patterns between the *P* and runoff or the *sc_PDSI_pm* and runoff would suggest that the change patterns in both fields are likely to be real, as the chance for the errors in *P* and streamflow to induce similar trend patterns is low.

Although some regional disagreements are evident between the *P* and runoff changes (Fig. 2), e.g., over Siberia where the runoff increases may have partly resulted from reduced evapotranspiration and thawing permafrost (Adam and Lettenmaier 2008), overall the three different measures of drought all suggest widespread drying from 1950 to 2012 over Africa, East and South Asia, eastern Australia, central South America, southern Europe and the Middle East, and eastern and western Canada; while wetting trends are apparent the central U.S., northern Europe, Argentina, northwestern Australia, and some other regions (Fig. 2). As shown previously (Dai 2013b; Dong and Dai 2015), precipitation trends since the 1950s (and especially since the 1990s) over southwestern North America, eastern Australia, southern

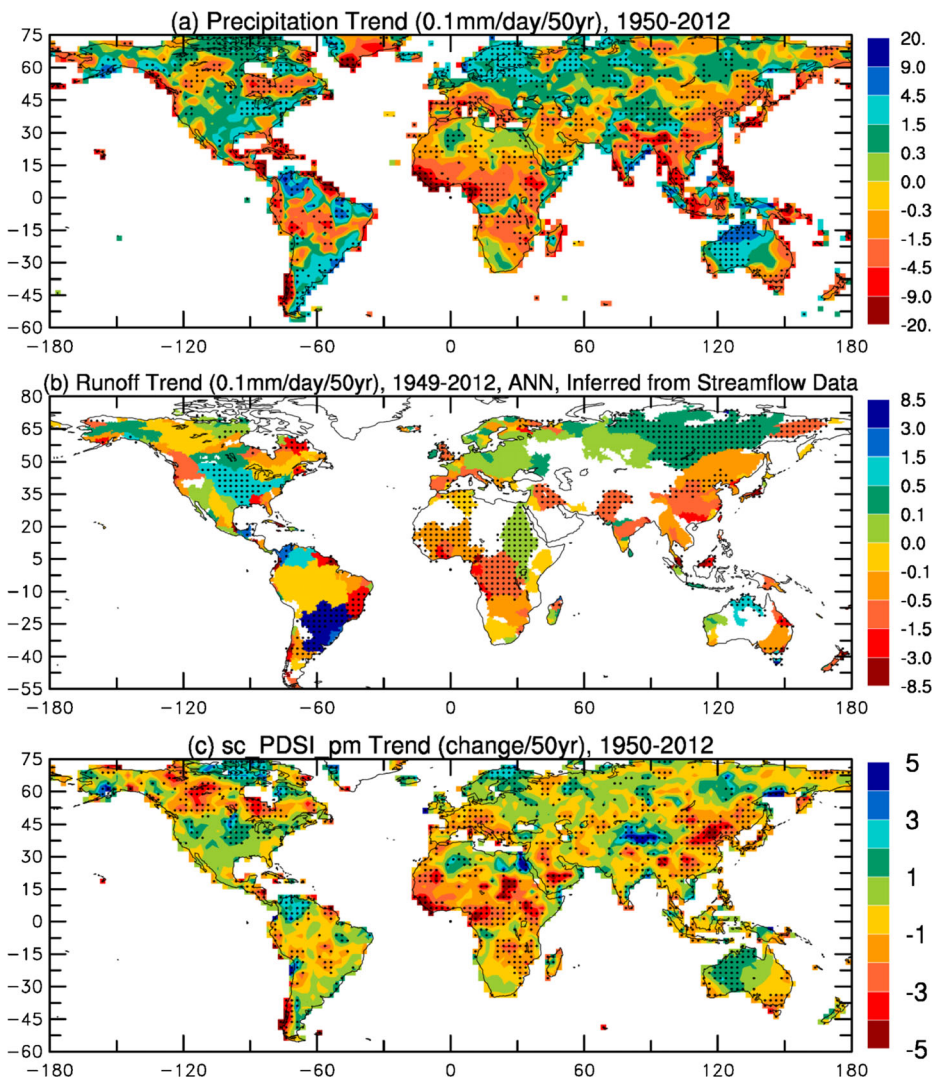


Fig. 2 Long-term trend in annual (a) precipitation, (b) basin-mean runoff (inferred from streamflow gauge records of the water year from October of the previous year to September of the current year), and (c) sc_PDSI_pm during 1950–2012. Blank land areas in (b) do not have runoff into the oceans or do not have enough observations. The merged CPC (for 1948–1978 from Chen et al. 2002) and GPCP v2.2 (for 1979–present) precipitation data are used for (a) and (c). Panels (a) and (c) differ slightly if other precipitation datasets are used. A negative trend in sc_PDSI_pm represents drying. The stippling indicates the trend is statistically significant at the 5 % level

Africa, Argentina, and other regions are strongly influenced by the decadal to multi-decadal oscillations in Pacific sea surface temperatures (SSTs), namely the Inter-decadal Pacific Oscillation (IPO), which is a natural mode of internal climate variability (Liu 2012). Thus, many of the regional trends shown in Fig. 2 have partly resulted from natural climate variations such as the IPO, rather than entirely being caused by recent global warming.

The drying trend in the sc_PDSI_pm (Fig. 2c) is more widespread (over $9.259 \times 10^7 \text{ km}^2$) than the decreasing precipitation trend (Fig. 2a, over $8.467 \times 10^7 \text{ km}^2$), as precipitation only

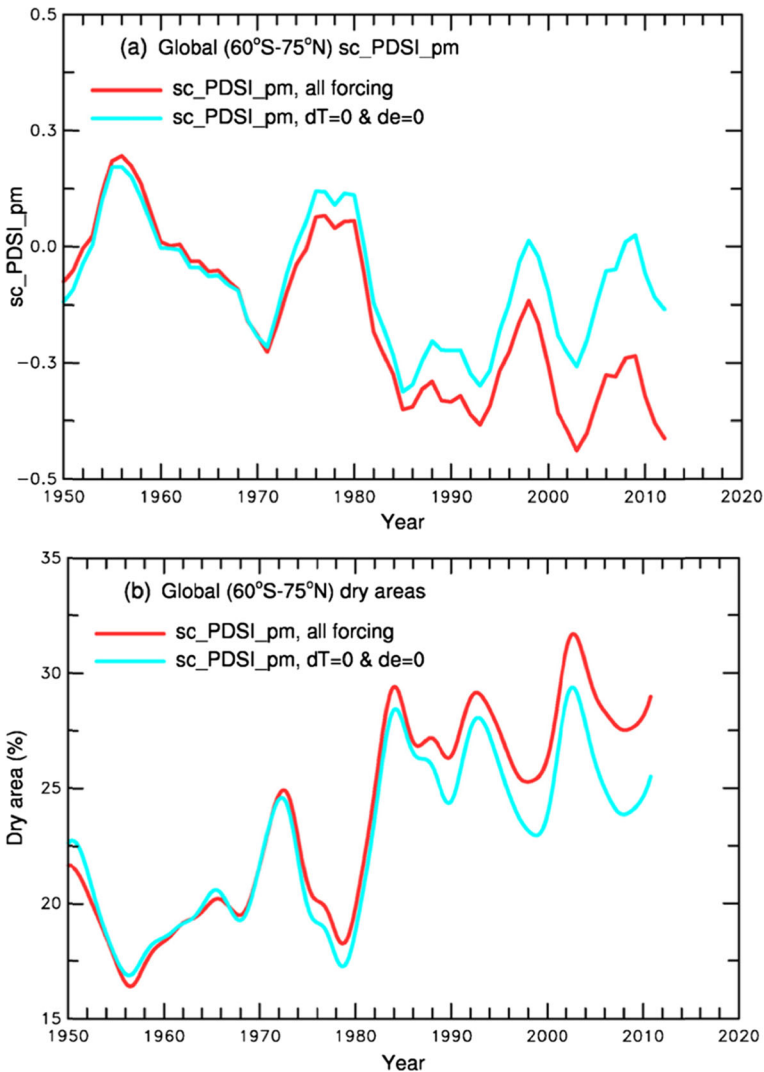
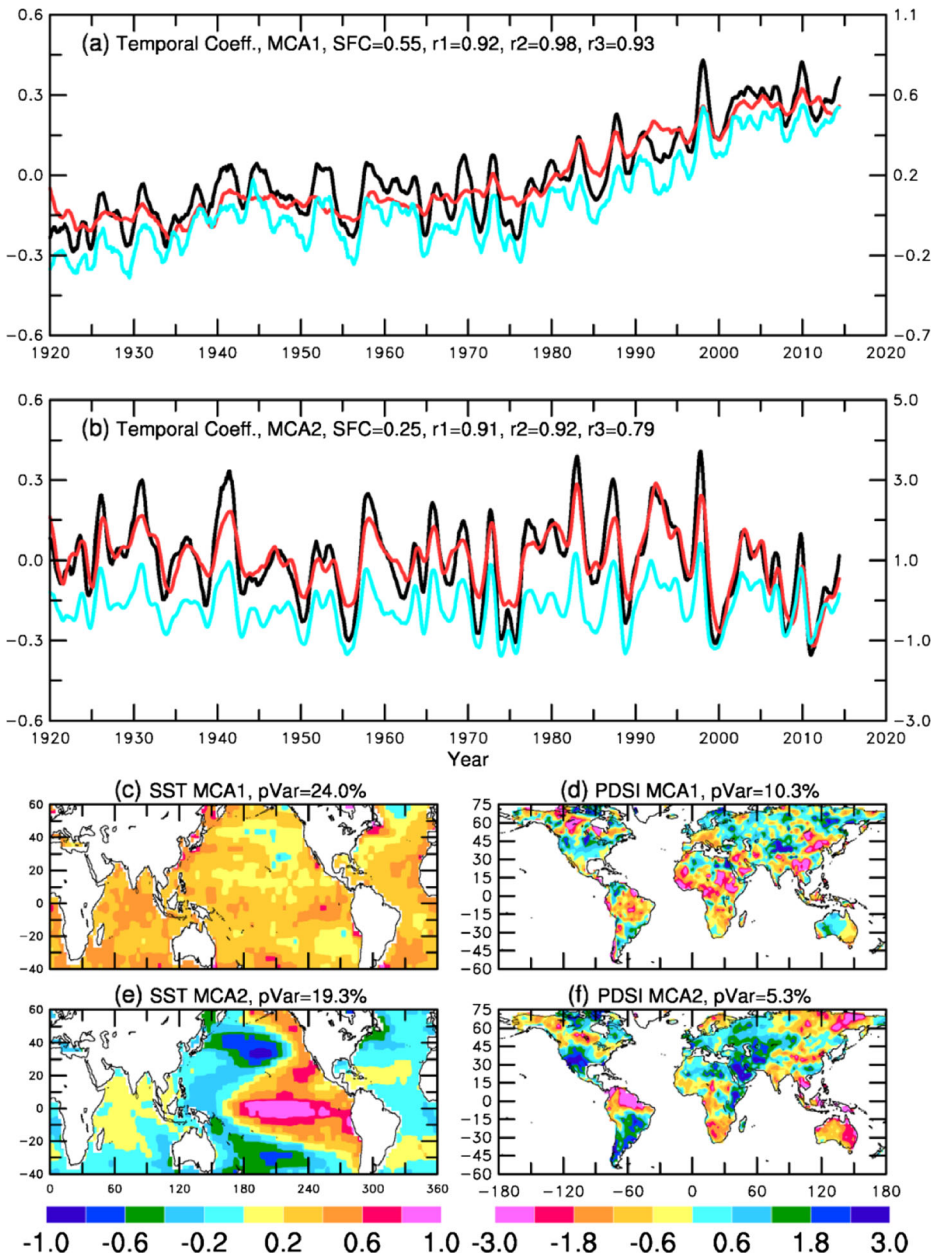


Fig. 3 Globally (60°S-75°N) averaged and 5-year smoothed time series of (a) sc_PDSI_pm and (b) percentage dry areas from 1950 to 2014 calculated using the DaiP precipitation data and other meteorological forcing data from the CRU TS3.22 and 20CR (see section 2). The dry area for a given month is defined as any 2.5° grid box whose monthly sc_PDSI_pm is below its 20th percentile of the 1950–1979 base period. The red lines are for the case where all changes in the forcing data are included, while the blue lines are for the case where surface air temperature and vapor pressure were kept constant but all other changes are included. The slope (p -value, i.e., attained significance) is -0.76 per century ($p < 0.01$) for the red line and -0.29 per century ($p = 0.029$) for the blue line in (a), and is 21.2 % per century ($p < 0.01$) for the red line and 14.5 % per century ($p < 0.01$) for the blue line in (b). Autocorrelation was considered in computing the p -value by reducing the effective degrees of freedom based on Zhao and Khalil (1993)

reflects the supply of water to the surface while sc_PDSI_pm also accounts for changes in atmospheric demand for moisture from the surface. With rising surface air temperatures (Fig. S3a), atmospheric demand for moisture increases during the most recent decades (Fig. S3f), which leads to drier surfaces as reflected by the sc_PDSI_pm trend (Fig. 2c).



This drying effect from rising temperatures is shown more clearly in Fig. 3, in which the globally (60°S - 75°N) averaged sc_PDSI_pm from two cases is compared: one includes all changes (red line) and the other includes all but the temperature and vapor pressure changes (blue line). The difference between these two cases illustrates the direct impact of surface warming and the associated increases in surface vapor pressure deficit (VPD, Figs. S3-S6) on the sc_PDSI_pm mainly through their influences on PET.

Fig. 4 Temporal (a–b, black for SST, red for *sc_PDSI_pm*) and spatial (c–f) patterns of the two leading modes from a maximum covariance analysis (MCA, Bretherton et al. 1992) of the observed SST (from HadSST3, Rayner et al. 2006) and the DaiP-based *sc_PDSI_pm*. Panels (a), (c) and (d) are for the first MCA mode (MCA1); and panels (b), (e) and (f) are for the second MCA mode (MCA2). Thirteen-point moving-averaged monthly data were used in the analysis. The blue line in (a) is the global-mean surface temperature obtained from the Climate Research Unit (CRU, <http://www.cru.uea.ac.uk/cru/data/temperature/HadCRUT4-gl.dat>), and the blue line in (b) is the observed Niño3.4 SST index (right-side ordinate) obtained from <http://www.esrl.noaa.gov/psd/forecasts/sstlim/Globalsst.html> (for 1950–2010) and from http://www.cgd.ucar.edu/cas/catalog/climind/TNI_N34/index.html#Sec5 (for pre-1950 years, rescaled to match the NOAA index over the 1950–2007 period). In (a–b), SFC is the squared fractional covariance explained by the MCA mode and the r_1 , r_2 , and r_3 are the correlation coefficients between, respectively, the black and red, black and blue, red and blue lines. $pVar$ is the percentage variance explained by the MCA mode in (c–f). The corresponding MCA modes depict the statistically associated temporal and spatial patterns in the SST and *sc_PDSI_pm* fields. The product of the temporal and spatial coefficients at a given location is the SST or *sc_PDSI_pm* anomaly represented by the MCA mode

Figure 3 shows that the recent increases in T and VPD have enhanced the downward trend in global-mean *sc_PDSI_pm* from $-0.29/\text{century}$ (significant at the 5 % level) to $-0.76/\text{century}$ (significant at the 1 % level) and the upward trend in global drought area from 14.5 % to 21.2 % per century (both significant at the 1 % level). Global drought areas have increased from about 20 % (of global land area) during 1950–1979 to about 30 % since the late 1990s, with an increasingly large contribution from the effect of surface warming and VPD increases (Fig. 3b). The VPD increases derived from the CRU data are qualitatively consistent with those projected by CMIP5 models under a warming climate (Scheff and Frierson 2014; Zhao and Dai 2015). Thus, the large surface warming and the associated VPD increases since the 1980s have substantially enhanced the drying over global land and increased the drought areas during the last thirty years.

Given the well-documented influences of ENSO- (Dai and Wigley 2000) and IPO-related (Dai 2013b; Dong and Dai 2015) SST variations on land precipitation and temperature, we expect significant influences of SSTs on land aridity. To further quantify this, we performed a maximum covariance analysis (MCA, Bretherton et al. 1992) of the 13-point smoothed monthly SST and *sc_PDSI_pm* fields from 1920 to 2014 to extract the statistically associated leading patterns in the SST and *sc_PDSI_pm* fields. The first mode for SST shows a temporal evolution that is strongly correlated with the global-mean surface temperature ($r = 0.99$, blue line in Fig. 4a), with the SST pattern (Fig. 4c) showing warming over almost all oceans from 1920 to 2014. Thus, this mode represents global warming. The associated mode for *sc_PDSI_pm* also shows a time series (red line in Fig. 4a) that is highly correlated with the global-mean surface temperature ($r = 0.90$). However, the spatial pattern for this mode in *sc_PDSI_pm* (Fig. 4d) contains large internal variations that are also reflected in its trend map (Fig. 2c), and it does not match well the *sc_PDSI_pm* change pattern in response to GHG-induced warming (Zhao and Dai 2015). Dai (2013a) suggested that this mis-match on regional scales is likely due to large sampling noise in the MCA mode; that is, the GHG-induced drying trend is not yet detectable on regional scales given the large internal variability, although it is also possible that some of the CMIP5 change patterns may be incorrect, thereby contributing to the discrepancies.

The second MCA mode (Figs. 4b, 4e–f) represents the ENSO- and IPO-related SST variations primarily in the Pacific, since its temporal coefficients are highly correlated with the Niño3.4 SST index (blue line in Fig. 4b) and its SST pattern (Fig. 4e) resembles the typical ENSO and IPO mode (Dai 2013b; Dong and Dai 2015). After averaging the data with 9-year running mean, the MCA2 (Fig. S7) shows that multi-decadal *sc_PDSI_pm* variations, which affect its long-term trends, are most pronounced over Southwest North America, central South

America, and the Middle East (with drier conditions when the eastern Pacific is cooler than normal), and also over West Africa, parts of eastern Asia and northern North America (with drier conditions when the eastern Pacific is warmer than normal). Interestingly, Australia, southern Africa and northern South America show muted response to multi-decadal SST anomalies compared with those shown in Fig. 4f.

In particular, MCA2 induces an apparent downward trend since the early 1990s associated with the IPO phase change (Figs. 4b and S7b). This apparent trend represents a cooling (warming) in the central and eastern Pacific (western Pacific) during the last 20 years (Figs. 4e and S7e), and a drying trend since the 1990s over many land areas such as Southwest North American, central and southern South America, the Middle East and northern Africa (Fig. S7f). The *sc_PDSI_pm* patterns shown in Fig. 4f are broadly consistent with the ENSO- and IPO-induced precipitation anomaly patterns (Dai and Wigley 2000; Dong and Dai 2015). Thus, the second MCA mode for *sc_PDSI_pm* (Figs. 4b and 4f) represents the impacts of ENSO- and IPO-induced SST variations on land aridity and drought, and these impacts are large for many regions in dark blue or red color in Fig. 4f.

5 Comparison with pan evaporation trends

To assess whether our estimated PET trends (and thus the PDSI trends) are consistent with previously reported trends in pan evaporation (Epan, McVicar et al. 2012), we show the trend maps for PET and its key drivers in Figs. S4–S6 for three different periods from 1950 to 2012, 1955–2000, and 1980–2012 (so that the PET trends can be roughly compared with the Epan trends over various periods). These figures show that our estimated PET trends are negative or close to zero over most of the contiguous U.S. for all the three periods (consistent with the Epan trends), near-zero over most China (except its Northeast) from 1955 to 2000, and positive from 1980 to 2012 over most China (consistent with the positive Epan trends for 1992–2007 from study #19 in Table 5 of McVicar et al. 2012). The positive PET trend over Northeast China results mainly from the positive net radiation trend in our forcing data (Fig. S5), which is likely unrealistic as increasing air pollution has dimmed surface solar radiation over that region but this effect was ignored here. Over India, our estimated PET trend from 1980 to 2012 is negative or close to zero except northern India, where our PET shows positive values. Over Australia and New Zealand, our PET shows mostly negative or near zero trends from 1955 to 2000, but large positive trends from 1980 to 2012 over northern and central Australia. Globally, our land PET does not show a clear upward trend before the 1990s (Fig. S3f).

Wang et al. (2012) calculated the PET using station weather reports and the Penman-Monteith equation, and showed that PET during 1982–2008 over Asia, North America and Europe exhibits mostly decadal variations rather than monotonic trends, and that water vapor deficit has the largest influence on PET. Given the uncertainties in our forcing data (especially solar radiation) and the broad consistency between our PET and the Epan trends (and the PET of Wang et al. 2012), we conclude that our estimated PET is consistent with most of the reported Epan trends. Thus, our PDSI drying trends since 1950, which are supported by the precipitation and runoff trends (Fig. 2), are consistent with most of the reported Epan trends. Since the trend in global PET up to the 1990s is small (Fig. S3), the PDSI drying trends since 1950 result mainly from precipitation decreases (Fig. 2), although increasing PET since the 1990s is also a significant contributor for the recent period.

6 Summary

We have examined the main uncertainty sources in estimating historical drying trends based on *sc_PDSI_pm* or *PDSI_pm*, and evaluated the *sc_PDSI_pm* trend with observed changes in precipitation and runoff for assessing historical drought changes. The main findings are summarized as follows.

- 1) The GPCP V6 and GPCP v2.2 precipitation data sets are likely to be more reliable than other (including CRU) datasets for estimating global land precipitation changes for the period since the 1990s, primarily due to the fact that too few rain-gauges were included in the other datasets for the recent decades.
- 2) Updated records of precipitation, streamflow and the calculated *sc_PDSI_pm* show spatially consistent patterns of drying during 1950–2012 over most Africa, East and South Asia, southern Europe, eastern Australia, and many parts of the Americas. They confirm the findings by Dai et al. (2004); Dai (2011a, 2011b) and Dai (2013a), while the “little drying” conclusion made by Sheffield et al. (2012) solely based on their calculated *PDSI_pm* is likely influenced by spurious changes in their precipitation, radiation and wind forcing data.
- 3) Our estimated PET trends are broadly consistent with most of the reported trends in pan evaporation (McVicar et al. 2012), with negative or small trends over the United States, China and many other regions and no trends in global-mean PET from the 1950s to the 1980s. However, since the 1980s, rapid warming and associated VPD increases have significantly enhanced drying over global land. These drying effects are consistent with climate model projections, even though the effects of man-made aerosols were not included in our forcing data.
- 4) An MCA analysis suggests that Pacific SST variations associated with ENSO and IPO, respectively, have large influences on multi-year variations and multi-decadal trends in drought over many land areas, such as southwestern North America, South America, West and South Asia, southern and northern Africa, southern Europe, and Australia. This large internal variability still dominates over GHG-induced drought trends over these regions.

Acknowledgments We thank J. Scheff, G. van der Schrier and another anonymous reviewer for constructive review comments. This study was supported by the National Key Basic Research Program of China (Grant No.2012CB956203), the U.S. National Science Foundation (Grant #AGS-1353740), U.S. Department of Energy’s Office of Science (Award #DE-SC0012602), and the U.S. National Oceanic and Atmospheric Administration (Award #NA15OAR4310086).

References

- Adam JC, Lettenmaier DP (2008) Application of new precipitation and reconstructed streamflow products to streamflow trend attribution in northern Eurasia. *J Clim* 21:1807–1828
- Barriopedro D, Gouveia CM, Trigo RM, Wang L (2012) The 2009/10 drought in China: possible causes and impacts on vegetation. *J Hydrometeorol* 13:1251–1267
- Bretherton CS, Smith C, Wallace JM (1992) An intercomparison of methods for finding coupled patterns in climate data. *J Clim* 5:541–560

- Burke EJ, Brown SJ, Christidis N (2006) Modeling the recent evolution of global drought and projections for the twenty-first century with the hadley centre climate model. *J Hydrometeorol* 7:1113–1125
- Cook BI, Smerdon JE, Seager R, Coats S (2014) Global warming and twenty-first century drying. *Clim Dyn* 43: 2607–2627
- Compo GP et al. (2011) The twentieth century reanalysis project. *Q J R Meteorol Soc* 137:1–28
- Dai A (2011a) Drought under global warming: a review. *WIREs Clim Change* 2:45–65
- Dai A (2011b) Characteristics and trends in various forms of the palmer drought severity index during 1900–2008. *J Geophys Res* 116:D12115
- Dai A (2013a) Increasing drought under global warming in observations and models. *Nat Clim Chang* 3:52–58
- Dai A (2013b) The influence of the inter-decadal Pacific oscillation on U.S. precipitation during 1923–2010. *Clim Dyn* 41:633–646
- Dai A (2016) Historical and future changes in streamflow and continental runoff: A review. AGU Monograph entitled “*Terrestrial Water Cycle and Climate Change: Natural and Human-induced Impacts*” (eds by Tang Q et al.), in press.
- Dai A, Fung IY, Del Genio AD (1997) Surface observed global land precipitation variations during 1900–1988. *J Clim* 10:2943–2962
- Dai A, Trenberth KE, Karl TR (1998) Global variations in droughts and wet spells: 1900–1995. *Geophys Res Lett* 25:3367–3370. doi:10.1029/98GL52511
- Dai A, Wigley TML (2000) Global patterns of ENSO-induced precipitation. *Geophys Res Lett* 27:1283–1286
- Dai A, Trenberth KE, Qian T (2004) A global dataset of palmer drought severity index for 1870–2002: relationship with soil moisture and effects of surface warming. *J Hydrometeorol* 5:1117–1130. doi:10.1175/JHM-386.1
- Dai A, Qian T, Trenberth KE, Milliman JD (2009) Changes in continental freshwater discharge from 1949 to 2004. *J Clim* 22:2773–2791
- Dong B, Dai A (2015) The influence of the inter-decadal Pacific oscillation on temperature and precipitation over the globe. *Clim Dyn* 45:2667–2681. doi:10.1007/s00382-012-1446-5
- Feng S, Fu Q (2013) Expansion of global dry lands under warming climate. *Atmos Chem Phys* 13:10081–10094
- Hoerling M, Kumar A, Dole R, Nielsen-Gammon JW, Eischeid J, Perlwitz J, Quan X-W, Zhang T, Pegion P, Chen M (2012) Anatomy of an extreme event. *J Clim* 26:2811–2832. doi:10.1175/JCLI-D-12-00270.1
- IPCC (2007) *Climate change 2007: the physical science basis* (eds Solomon S et al.). Cambridge University Press, Cambridge.
- IPCC (2013) *Climate Change 2013: The Physical Science Basis* (eds Stocker TE et al.). Cambridge University Press, Cambridge.
- Lewis S, Brando P, Phillips O, van der Heijden G, Nepstad D (2011) The 2010 Amazon drought. *Science* 331: 554–554
- Liu ZY (2012) Dynamics of interdecadal climate variability: a historical perspective. *J Clim* 25:1963–1995
- Lyon B, DeWitt DG (2012) A recent and abrupt decline in the east African long rains. *Geophys Res Lett* 39: L02702. doi:10.1029/2011GL050337
- Marengo JA, Nobre CA, Tomasella J, Oyama MD, deOliveira GS, de Oliveira R, Camargo H, Alves LM, Brown IF (2008) The drought of Amazonia in 2005. *J Clim* 21:495–516
- McGrath GS, Sadler R, Fleming K, Tregoning P, Hinz C, Veneklaas EJ (2012) Tropical cyclones and the ecohydrology of Australia’s recent continental-scale drought. *Geophys Res Lett* 39:L03404. doi:10.1029/2011GL050263
- McVicar TR et al. (2012) Global review and synthesis of trends in observed terrestrial near-surface wind speeds: implications for evaporation. *J Hydrol* 416–417:182–205
- Mishra AK, Singh VP (2010) A review of drought concepts. *J Hydrol* 391:202–216. doi:10.1016/j.jhydrol.2010.07.012
- Myhre, G., et al, 2013: Anthropogenic and natural radiative forcing. *Climate Change 2013: The Physical Science Basis*, T. F. Stocker et al., Eds., Cambridge University Press, 659–740, doi:10.1017/CBO9781107415324.018.
- Palmer WC (1965) Meteorological drought. US Weather Bureau Research Paper 45: 55 pp
- Peterson T, Stott P, Herring S (2012) Explaining extreme events of 2011 from a climate perspective. *Bull Am Meteorol Soc* 93:1041–1067
- Prudhomme C et al. (2014) Hydrological droughts in the twenty-first century, hotspots and uncertainties from a global multimodel ensemble experiment. *Proc Natl Acad Sci U S A* 111:3262–3267. doi:10.1073/pnas.1222473110
- Scheff J, Frierson D (2014) Scaling potential evapotranspiration with greenhouse warming. *J Clim* 27:1539–1558. doi:10.1175/JCLI-D-13-00233.1
- Scheff J, Frierson D (2015) Terrestrial aridity and its response to greenhouse warming across CMIP5 climate models. *J Clim* 28:5583–5600

- Seager R et al. (2007) Model projections of an imminent transition to a more arid climate in southwestern North America. *Science* 316:1181–1184
- Sheffield J, Wood EF (2008) Projected changes in drought occurrence under future global warming from multi-model, multi-scenario, IPCC AR4 simulations. *Clim Dyn* 31:79–105
- Sheffield J, Wood EF, Roderick ML (2012) Little change in global drought over the past 60 years. *Nature* 491(7424):435–438. doi:10.1038/nature11575
- Sun C, Yang S (2012) Persistent severe drought in southern China during winter and spring 2011: large-scale circulation patterns and possible impacting factors. *J Geophys Res* 117:D10112. doi:10.1029/2012JD017500
- Swenson, SC (2012) GRACE monthly land water mass grids NETCDF RELEASE 5.0. Ver. 5.0. PO.DAAC, CA, USA. Dataset accessed on 2016–02–24 at doi:10.5067/TELND-NC005.
- Taylor IH, Burke E, McColl L, Falloon PD, Harris GR, McNeall D (2013) The impact of climate mitigation on projections of future drought. *Hydrol Earth Syst Sci* 17:2339–2358. doi:10.5194/hess-17-2339-2013
- Trenberth KE, et al (2007) Observations: Surface and Atmospheric Climate Change. *Climate Change 2007: The Physical Science Basis*, S. Solomon, D. Qin, M. Manning, Z. Chen, M. Marquis, K.B. Averyt, M. Tignor, and H.L. Miler, Ed., Cambridge University Press, 235–336.
- Trenberth KE, Dai A, van der Schrier G, Jones PD, Barichivich J, Briffa KR, Sheffield J (2014) Global warming and changes in drought. *Nat Clim Chang* 4:17–22
- van der Schrier G, Efthymiadis D, Briffa KR, Jones PD (2007) European alpine moisture variability for 1800–2003. *Int J Climatol* 27:415–427. doi:10.1002/joc.1411
- van der Schrier G, Jones PD, Briffa KR (2011) The sensitivity of the PDSI to the Thornthwaite and penman-Monteith parameterizations for potential evapotranspiration. *J Geophys Res Atmos* 116:D03106. doi:10.1029/2010JD015001
- van der Schrier G, Barichivich J, Briffa KR, Jones PD (2013) A scPDSI-based global data set of dry and wet spells for 1901–2009. *J Geophys Res Atmos* 118:4025–4048. doi:10.1002/jgrd.50355
- Wang GL (2005) Agricultural drought in a future climate: results from 15 global climate models participating in the IPCC 4th assessment. *Clim Dyn* 25:739–753
- Wang K, Dickinson RE, Liang S (2012) Global atmospheric evaporative demand over land from 1973 to 2008. *J Clim* 25:8353–8361
- Wehner M, Easterling DR, Lawrimore JH, Heim RR, Vose RS, Santer BD (2011) Projections of future drought in the continental United States and Mexico. *J Hydrometeorol* 12:1359–1377
- Wei K, Wang L (2013) Reexamination of the aridity conditions in arid northwestern China for the last decade. *J Clim* 26:9594–9602
- Wells N, Goddard S, Hayes MJ (2004) A self-calibrating palmer drought severity index. *J Clim* 17:2335–2351
- Wilhite DA (2000) Drought as a natural hazard: concepts and definitions. In: Wilhite DA (ed) *Droughts: a global assessment*. Routledge, New York, pp. 3–18
- Williams AP, Seager R, Abatzoglou JT, Cook BI, Smerdon JE, Cook ER (2015) Contribution of anthropogenic warming to California drought during 2012–2014. *Geophys Res Lett* 42:6819–6828. doi:10.1002/2015GL064924
- Zhai J, Su B, Krysanova V, Vetter T, Gao C, Jiang T (2010) Spatial variation and trends in PDSI and SPI indices and their relation to streamflow in 10 large regions of China. *J Clim* 23:649–663
- Zhao T, Dai A (2015) The magnitude and causes of global drought changes in the twenty-first century under a low–low–moderate emissions scenario. *J Clim* 28:4490–4512
- Zhao T, Dai A (2016) Uncertainties in historical changes and future projections of drought. Part II: model-simulated historical and future drought changes. *Clim Change* (this issue).
- Zhao W, Khalil MAK (1993) The relationship between precipitation and temperature over the contiguous United States. *J Clim* 6:1232–1236